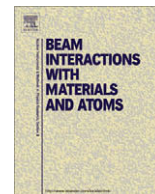




Contents lists available at ScienceDirect

Nuclear Instruments and Methods in Physics Research B

journal homepage: www.elsevier.com/locate/nimb

Radiation damage in ZnO ion implanted at 15 K

E. Wendler^{a,*}, O. Bilani^a, K. Gärtner^a, W. Wesch^a, M. Hayes^b, F.D. Auret^b, K. Lorenz^c, E. Alves^c^a Institut für Festkörperphysik, Friedrich-Schiller-Universität Jena, Max-Wien-Platz 1, 97743 Jena, Germany^b Department of Physics, University of Pretoria, Pretoria 0002, South Africa^c Instituto Tecnológico e Nuclear, Estrada Nacional 10, 2686 Sacavém, Portugal

ARTICLE INFO

Article history:
Available online xxxxxPACS:
61.05.Np
61.80.Jh
61.82.MsKeywords:
ZnO
Zinc oxide
Ion implantation
Radiation damage

ABSTRACT

Commercial O-face (0 0 0 1) ZnO single crystals were implanted with 200 keV Ar ions. The ion fluences applied cover a wide range from 5×10^{11} to $7 \times 10^{16} \text{ cm}^{-2}$. The implantation and the subsequent damage analysis by Rutherford backscattering spectrometry (RBS) in channelling geometry were performed in a special target chamber at 15 K without changing the target temperature of the sample. To analyse the measured channelling spectra the computer code DICADA was used to calculate the relative concentration of displaced lattice atoms.

Four stages of the damage evolution can be identified. At low ion fluences up to about $2 \times 10^{13} \text{ cm}^{-2}$ the defect concentration increases nearly linearly with rising fluence (stage I). There are strong indications that only point defects are produced, the absolute concentration of which is reasonably given by SRIM calculations using displacement energies of $E_d(\text{Zn}) = 65 \text{ eV}$ and $E_d(\text{O}) = 50 \text{ eV}$. In a second stage the defect concentration remains almost constant at a value of about 0.02, which can be interpreted by a balance between production and recombination of point defects. For ion fluences around $5 \times 10^{15} \text{ cm}^{-2}$ a second significant increase of the defect concentration is observed (stage III). Within stage IV at fluences above 10^{16} cm^{-2} the defect concentration tends again to saturate at a level of about 0.5 which is well below amorphisation. Within stages III and IV the damage formation is strongly governed by the implanted ions and it is appropriate to conclude that the damage consists of a mixture of point defects and dislocation loops.

© 2009 Elsevier B.V. All rights reserved.

1. Introduction

ZnO is a wide-gap material exhibiting a direct band gap, which makes it a promising and strongly studied material for electronic and optoelectronic devices (see e.g. [1–3]). In device fabrication ion implantation is an approved technology. Therefore, the investigation of ion-beam induced effects is both of scientific and technological importance and has attracted much interest in recent years (see e.g. [4–6]). In this paper we concentrate on the primary damage formation over a broad range of ion fluences and at very low temperatures at which thermal effects can be widely excluded.

2. Experimental conditions

A commercial O-face (0 0 0 1) ZnO single crystal was stepwise implanted at 15 K with 200 keV Ar ions. After each implantation step immediate defect analysis was performed using Rutherford backscattering spectrometry (RBS) in a channelling configuration with 1.4 MeV He ions and a backscattering angle of 170° . The experiments done in a special target chamber at the Institut für

Festkörperphysik in Jena, allow for implantation and subsequent ion beam analysis without changing the target temperature or the environment of the sample [7].

In the first series a maximum ion fluence of $N_i = 2.5 \times 10^{14} \text{ cm}^{-2}$ was achieved. Then the sample was warmed to room temperature. To continue the experiments, the sample was cooled down again and in the second series a final ion fluence of $N_i = 7 \times 10^{16} \text{ cm}^{-2}$ was obtained.

From the energy spectra of backscattered ions the difference in minimum yield $\Delta\chi_{\min}$ is obtained by $\Delta\chi_{\min} = (Y_{\text{impl}} - Y_{\text{perf}})/Y_{\text{ra}}$ with Y_{perf} and Y_{impl} being the yield measured in channelling direction before and after the implantation, respectively, and Y_{ra} is the random yield. The quantity $\Delta\chi_{\min}$ versus the depth z is analysed with the help of the computer code DICADA [8]. With this code calculations can be done in two directions. First, for a given defect profile the resulting difference in minimum yield $\Delta\chi_{\min}(z)$ can be calculated and, second, from a given $\Delta\chi_{\min}(z)$ the defect profile can be determined. In particular, defect profile means the relative concentration of uncorrelated displaced lattice atoms, n_{da} , versus depth z . Uncorrelated displaced lattice atoms result from point defects, point defect clusters or amorphous regions. The positions of the displaced lattice atoms are assumed to be randomly distributed within the lattice cell, i.e. there exist no preferred positions in the lattice cell.

* Corresponding author. Fax: +49 (0)3641 947302.
E-mail address: elke.wendler@uni-jena.de (E. Wendler).

The defect profiles following from the RBS analysis are compared with the distributions of the number of primary displacements per ion and unit length, N_{displ}^* , and the distributions of the implanted ions. Both quantities were calculated with SRIM2003 version [9]. The displacement energies of Zn and O were taken to be 65 and 50 eV, respectively, (see e.g. [6]). The ion fluence N_I is recalculated in displacements per lattice atom, n_{dpa} , with $n_{\text{dpa}} = N_{\text{displ}}^* N_I / N_0$ ($N_0 = 8.3 \times 10^{22} \text{ cm}^{-3}$ atomic density of ZnO and $N_{\text{displ}}^* = 6.22 \times 10^7 \text{ cm}^{-1}$ at the maximum of the distribution).

3. Results and discussion

3.1. Fluence dependence

Fig. 1(a) shows a typical set of energy spectra of He ions backscattered from Ar implanted ZnO for ion fluences between 2×10^{15} and $7 \times 10^{16} \text{ cm}^{-2}$. The channelling yield does not reach the random level, which means that the implanted layers are not amorphised. From the resulting $\Delta\chi_{\text{min}}$ the relative concentration of displaced lattice atoms versus depth, $n_{\text{da}}(z)$, is calculated with DICADA, assuming the existence of randomly displaced lattice atoms. In the following text $n_{\text{da}}(z)$ is referred to as a defect or damage profile. The profiles resulting from the spectra given in Fig. 1(a) are plotted in Fig. 1(b). Behind the implanted layer (maximum range of primary displacements or ions is about 0.3 μm) n_{da} should reach zero, which is obviously not the case (see Fig. 1(b)). This finding suggests that the assumption of randomly displaced lattice

atoms made to extract the profiles from the spectra with the DICADA code is not correct. This is discussed in detail in Section 3.2.

To study the damage formation as a function of the ion fluence, the defect concentration n_{da} is averaged over a depth of 0.02 to 0.25 μm . The resulting values in Fig. 2 show that four stages of damage formation can be distinguished. Within the first stage the defect concentration increases steadily for fluences up to about $N_I \approx 5 \times 10^{13} \text{ cm}^{-2}$ and then reaches a plateau which is characterised by a relative defect concentration of about 0.02 (stage II). A second significant increase of the defect concentration occurs for ion fluences in the range of about $2 \times 10^{15} - 1 \times 10^{16} \text{ cm}^{-2}$ (stage III) followed again by a plateau-like region (stage IV). The line in Fig. 2 is calculated using a simplified version of the Hecking model (see [6,10]). Stage I can be related to the production of primary point defects by single ion impacts. When the collision cascades of individual ions start to overlap, point defects recombine and the balance between defect production and recombination yields an almost constant defect concentration over a wide range of ion fluences (stage II). The stages III and IV can be interpreted as to be due to the formation of a second type of (non-recombinable) defects (called clusters) up to a certain saturation value.

The small step in the experimental data at $2.5 \times 10^{14} \text{ cm}^{-2}$ arises from the slight annealing of point defects due to the intermediate warming of the sample (see Section 2). However, besides this step, the warming has no relevant effect on the subsequent damage formation. This is true, because this ion fluence is only 10% of that for significant cluster formation. For the sample implanted with $2.5 \times 10^{14} \text{ Ar cm}^{-2}$ about 55% of the defects produced at 15 K anneal out after warming to room temperature (and measurement at 15 K). This is in agreement with annealing studies on Er implanted [6] and electron irradiated ZnO [11] in the same range of temperatures. In the case of electron irradiation only point defects are formed. The similarity of the annealing behaviour indicates that for low ion fluences also in the Ar and Er implanted ZnO mainly point defects exist. This supports the interpretation of the stages I and II of the damage formation. An Er implanted sample with an ion fluence ranging at the beginning of stage III did not show any recovery of the lattice damage. This confirms the assumption that stable clusters of defects are produced in stage III.

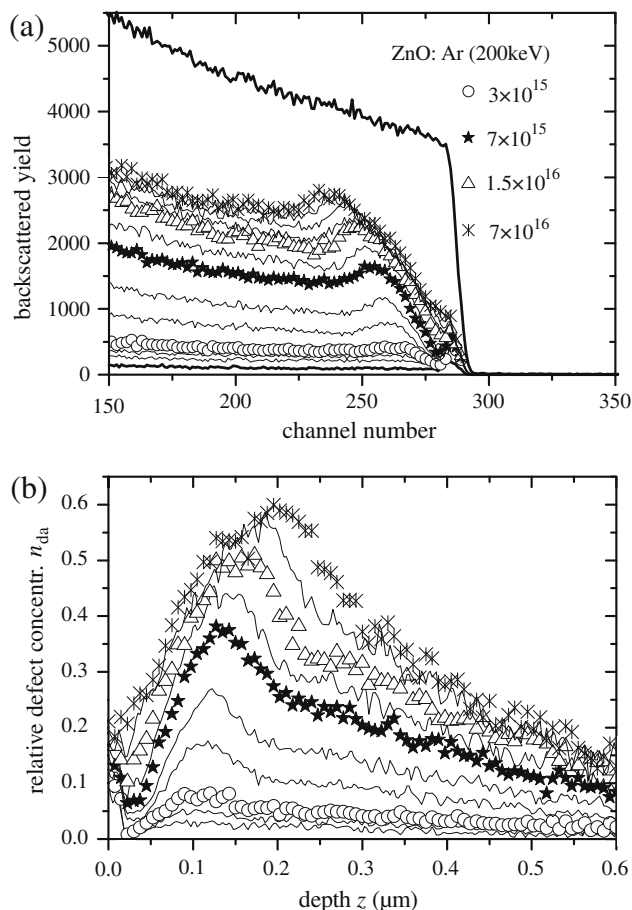


Fig. 1. Energy spectra of He ions backscattered from Ar implanted ZnO for various ion fluences (a), and (b) defect profiles resulting from the spectra in part (a) (for details see text). For clarity only some ion fluences are indicated with the values given in cm^{-2} .

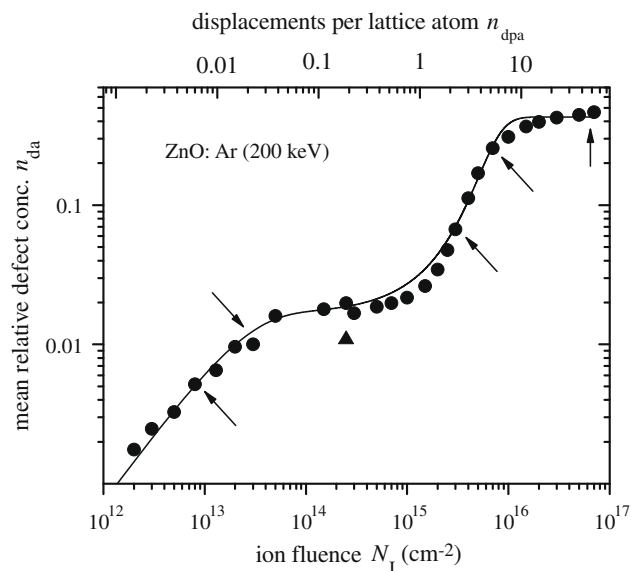


Fig. 2. Mean relative defect concentration n_{da} versus the ion fluence N_I . For convenience N_I is also recalculated in displacements per lattice atom n_{dpa} (upper scale, see Section 2). The triangle plots the value for $N_I = 2.5 \times 10^{14} \text{ cm}^{-2}$ measured at 15 K but after intermediate warming the sample to room temperature. The arrows indicate the fluences for which defect profiles are shown in Figs. 1(b) and 4.

So far only the mean defect concentration has been discussed. In order to obtain more information, the fluence dependence of the defect concentration is investigated separately at four different depths regions: at the depth of the maximum nuclear energy deposition (0.06–0.10 μm), at the depth of maximum ion concentration (0.11–0.15 μm), close to the surface (0–0.04 μm) and at the depth between surface and the maximum nuclear energy deposition (0.04–0.08 μm). The results are depicted in Fig. 3. The ion fluence N_I is recalculated in displacements per lattice atoms n_{dpa} (see Section 2). The corresponding values of N_{displ}^* are mean values over the same depths regions as used to average n_{da} . Fig. 3(a) shows the results for stages I and II for the first series of implants up to an ion fluence of $N_I = 2.5 \times 10^{14} \text{ cm}^{-2}$. In this case the data points from the different depth regions follow a uniform dependence. This means that the defect concentration produced is determined by the total number of displacements per unit volume, i.e. by the energy density deposited in collision processes. In contrast, for stages III and IV, a separate curve is found for each depth region (see Fig. 3(b)). With decreasing distance to the surface, the damage concentration decreases remarkably and, according to the SRIM results, the electronic energy loss increases. Therefore, a possible explanation of the decreasing damage concentration could be an ionisation-stimulated defect recovery during the implantation. This effect is well known also for other insulators and it is obvious to assume that it also occurs in ZnO. The highest damage production is observed in the maximum of ion distribution (see Fig. 3). This clearly points to a strong influence of the implanted ions on the cluster formation for ion fluences in stages III and VI.

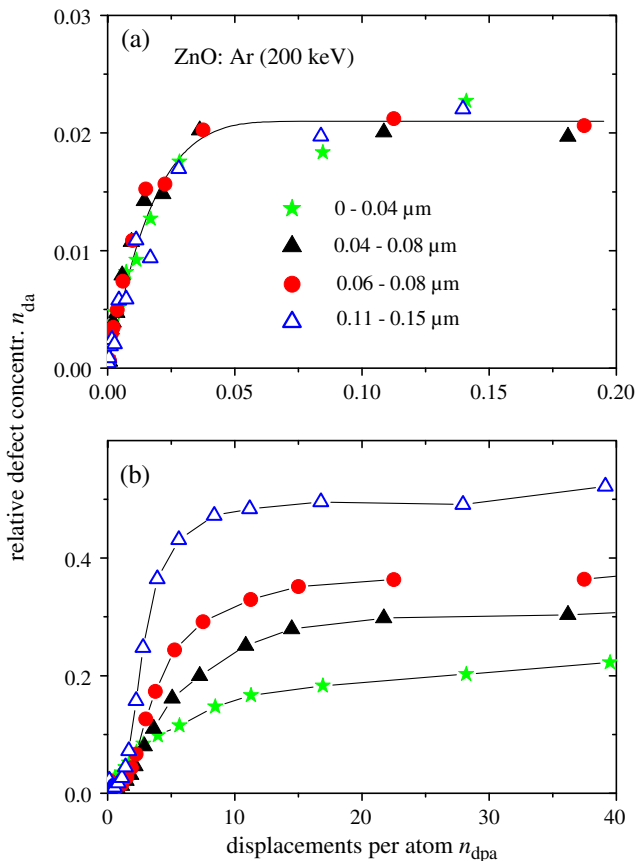


Fig. 3. Relative defect concentration n_{da} at different depth regions versus the number of displacements per lattice atoms n_{dpa} . The maximum nuclear energy deposition is at 0.06–0.10 μm and the maximum ion concentration at 0.11–0.15 μm .

3.2. Depth distribution of damage

Fig. 4 shows the defect profiles for two ion fluences ranging within ($N_I = 8 \times 10^{12} \text{ cm}^{-2}$) and at the end ($N_I = 3 \times 10^{13} \text{ cm}^{-2}$) of stage I (see the corresponding arrows in Fig. 2). Additionally the corresponding relative number of displacements per atom is given which were calculated with SRIM. Notice that the SRIM curves were not normalised but give the absolute results for the corresponding ion fluences. Despite the bad statistics, the depths range of the measured defects is in good agreement with the SRIM predictions. For $N_I = 8 \times 10^{12} \text{ cm}^{-2}$ ($n_{\text{dpa}} \approx 0.006$), the ion fluence within stage I, also the absolute values are reasonably represented by the calculations. The same result follows from Fig. 3(a): Up to $n_{\text{dpa}} = 0.01$ an almost linear dependence of $n_{\text{da}} = n_{\text{dpa}}$ is found. For $N_I = 3 \times 10^{13} \text{ cm}^{-2}$ ($n_{\text{dpa}} \approx 0.0225$) the calculated defect concentration is higher than the measured one. The reason for that is that this ion fluence ranges in the transition region to stage II (see Fig. 2), i.e. defect recombination already starts to occur. From these results the following conclusion can be drawn. At low energy densities deposited in nuclear processes (corresponding to $n_{\text{dpa}} < 0.01$, i.e. when each ion hits only crystalline material) the measured defect concentration can be represented by SRIM calculations with the displacement energies as given in Section 2. That is, no non-linear processes seem to occur within the collision cascades of individual ions. This behaviour is similar to that of GaN [12] and MgO [13] and may – at least to some extent – be related to the high displacement energies of 40–70 eV in these materials. In conventional semiconductors like Si, GaAs or InP the displacement energies are around 10–20 eV and strong non-linear processes occur at 15 K, i.e. the measured damage concentration is always much larger than the calculated one [14].

As already mentioned in Section 3.1, for higher ion fluences the assumption of randomly displaced lattice atoms, made to extract damage profiles from the measured spectra is not correct. To illustrate the effect of the kind of damage on the difference in minimum yield $\Delta\chi_{\text{min}}$ and the damage profiles, Fig. 5 plots some examples calculated for silicon with the DICADA code. Silicon was chosen because the calculation of extended defects is not included for compound crystals. Fig. 5(a) shows $\Delta\chi_{\text{min}}$ calculated with the DICADA code assuming three different situations: (1) a Gaussian distribution of randomly displaced lattice atoms with a maximum concentration of 0.5 at a depth of 0.1 μm , (2) a 0.25 μm thick layer containing a certain amount of dislocation loops and (3) the sum of (1) and (2). If only dislocation loops are assumed, $\Delta\chi_{\text{min}}$ does not show a peak because there is no contribution to direct backscattering of the

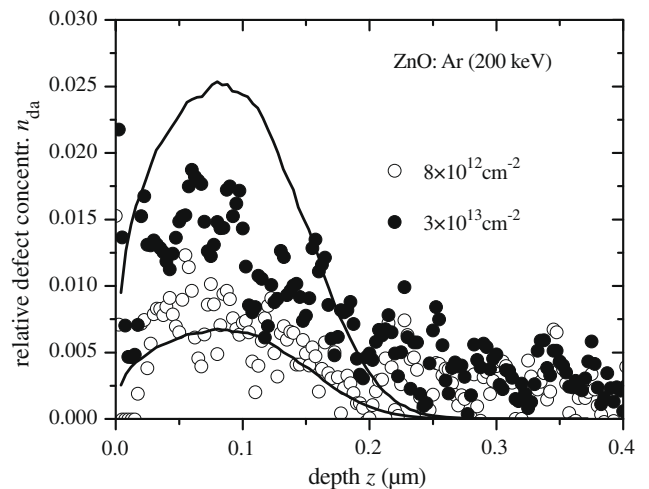


Fig. 4. Defect profiles $n_{\text{da}}(z)$ obtained for two low ion fluences. The symbols are the measurements and the lines are calculated with SRIM.

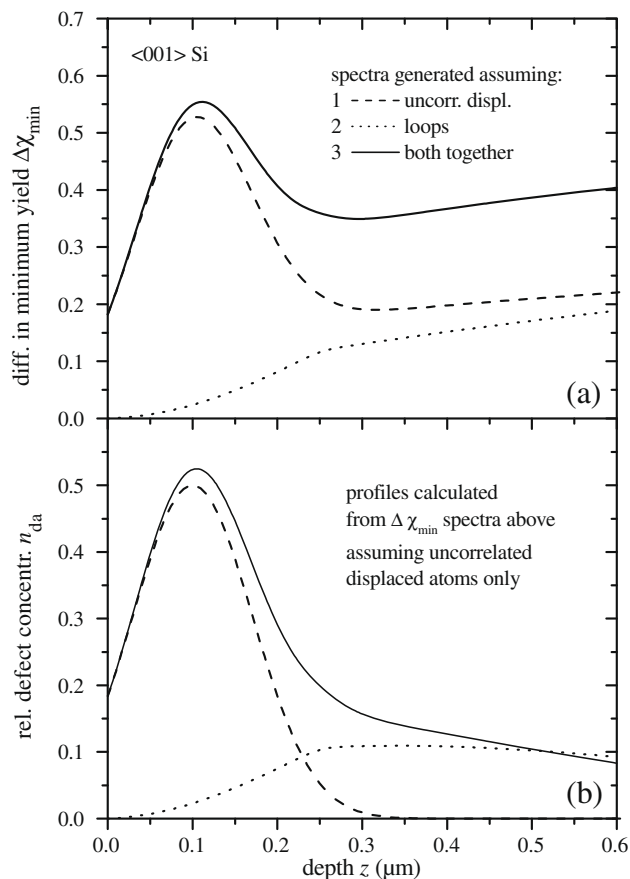


Fig. 5. (a) Difference in minimum yield $\Delta\chi_{\min}$ versus depth z calculated with DICADA for silicon assuming three different types of radiation damage. (b) Defect profiles following from the spectra in part (a). To extract the defect profiles, randomly displaced lattice atoms were assumed in all cases.

analysing ions. If both uncorrelated displaced atoms and dislocation loops exist within the implanted layer, the spectrum exhibits a peak due to the direct backscattering on the uncorrelated displaced atoms, but the yield behind that peak is much higher than for the case with only uncorrelated displaced atoms (see Fig. 5(a)). In a second step these $\Delta\chi_{\min}(z)$ curves were taken to extract a damage profile but with the assumption of uncorrelated displaced atoms only. The results are depicted in Fig. 5(b). In case (1) (only uncorrelated displaced atoms exist) one exactly obtains the Gaussian damage profile one has started with. In case (2) (only dislocation loops exist) the resulting damage profile is completely wrong: Dislocation loops

were assumed to exist only within the first $0.25 \mu\text{m}$, but the extracted profile extends far behind $0.6 \mu\text{m}$ (see Fig. 5(b)). And finally, such an artificial tail of damage is also observed in case (3) for which both types of damage were assumed to exist within the surface layer. Comparing that particular profile with those obtained for high-fluence implanted ZnO (Fig. 1(b)), a strong similarity is seen. It is therefore appropriate to conclude that the ion implanted ZnO layers implanted with ion fluences within stages III and IV contain a mixture of randomly displaced lattice atoms (i.e. clusters of point defects) and dislocation loops, even if implantation and defect analysis were done at 15 K.

4. Conclusion

ZnO belongs to the group of MgO and GaN, to which in our opinion also AlN and AlAs can be added [14]. In these materials SRIM calculations with displacement energies being measured or MD calculated, yield a reasonably good representation of the cross section of defect production per ion in crystalline material, measured at 15 K (thermal effects widely excluded). Only point defects are produced within a single ion impact in virgin material, which recombine when collision cascades of individual ions start to overlap, thus causing a saturation of the defect concentration at a rather low value (0.02–0.15 depending on the material). However, different effects occur in the various materials at higher ion fluences, when the implanted ions themselves start to play a dominating role in the process of damage formation.

References

- [1] D.C. Look, Mater. Sci. Eng. B 80 (2001) 383.
- [2] D.C. Look, B. Claffin, Ya.I. Alivov, J.S. Park, Phys. Stat. Sol. (a) 201 (2004) 2203.
- [3] S.J. Pearton, D.P. Norton, K. Ip, Y.W. Heo, T. Steiner, J. Vac. Sci. Technol. B 22 (2004) 932.
- [4] E. Alves, E. Rita, U. Wahl, J.G. Correia, T. Monteiro, J. Soares, C. Boemare, Nucl. Instr. and Meth. B 206 (2003) 1047.
- [5] F.D. Auret, S.A. Goodmann, M. Hayes, M.J. Legodi, H.A. van Laarhoven, D.C. Look, Appl. Phys. Lett. 79 (2001) 3074.
- [6] K. Lorenz, E. Alves, E. Wendler, O. Bilani, W. Wesch, M. Hayes, Appl. Phys. Lett. 87 (2005) 191904.
- [7] B. Breger, E. Wendler, W. Trippensee, Ch. Schubert, W. Wesch, Nucl. Instr. and Meth. B 174 (2001) 661.
- [8] K. Gärtner, Nucl. Instr. and Meth. B 227 (2005) 522.
- [9] J.F. Ziegler, J.P. Biersack, U. Littmark, The Stopping and Ranges of Ions in Solids, Pergamon, New York, 2003.
- [10] N. Hecking, K.F. Heidemann, E. TeKaas, Nucl. Instr. and Meth. B 15 (1986) 760.
- [11] Yu.V. Gorelkinskii, G.D. Watkins, Phys. Rev. B 69 (2004) 115212.
- [12] E. Wendler, A. Kamarou, E. Alves, K. Gärtner, W. Wesch, Nucl. Instr. and Meth. B 206 (2003) 1028.
- [13] E. Wendler, K. Gärtner, W. Wesch, Nucl. Instr. and Meth. B 266 (2008) 2872.
- [14] E. Wendler, W. Wesch, Advances in Solid State Physics, Vol. 44, Berlin, Heidelberg, New York, 2004. p. 339.